AIP | Journal of Applied Physics

Spectroscopic properties and radiation damage investigation of a diamond based Schottky diode for ion-beam therapy microdosimetry

C. Verona, G. Magrin, P. Solevi, V. Grilj, M. Jakšić, R. Mayer, Marco Marinelli, and G. Verona-Rinati

Citation: Journal of Applied Physics **118**, 184503 (2015); doi: 10.1063/1.4935525
View online: http://dx.doi.org/10.1063/1.4935525
View Table of Contents: http://scitation.aip.org/content/aip/journal/jap/118/18?ver=pdfcov
Published by the AIP Publishing

Spectroscopic properties and radiation damage investigation of a diamond based Schottky diode for ion-beam therapy microdosimetry

C. Verona,[1] G. Magrin,[2] P. Solevi,[2] V. Grilj,[3] M. Jakšić,[3] R. Mayer,[2] Marco Marinelli,[1] and G. Verona-Rinati[1]
[1]*INFN - Dipartimento di Ingegneria Industriale, Università di Roma "Tor Vergata," Roma, Italy*
[2]*EBG MedAustron Marie Curie-St. 5, 2700 Wiener Neustadt, Austria*
[3]*Ruder Boškovic Institute, Bijenicka cesta 54, P.O. Box 180, 10002 Zagreb, Croatia*

(Received 5 August 2015; accepted 29 October 2015; published online 12 November 2015)

In this work, a detailed analysis of the properties of a novel microdosimeter based on a synthetic single crystal diamond is reported. Focused ion microbeams were used to investigate the device spectropscopic properties as well as the induced radiation damage effects. A diamond based Schottky diode was fabricated by chemical vapor deposition with a very thin detecting region, about 400 nm thick (approximately 1.4 μm water equivalent thickness), corresponding to the typical size in microdosimetric measurements. A $200 \times 200\ \mu m^2$ square metallic contact was patterned on the diamond surface by standard photolithography to define the sensitive area. Experimental measurements were carried out at the Ruder Boškovic′ Institute microbeam facility using 4 MeV carbon and 5 MeV silicon ions. Ion beam induced charge maps were employed to characterize the microdosimeter response in terms of its charge collection properties. A stable response with no evidence of polarization or memory effects was observed up to the maximum investigated ion beam flux of about 1.7×10^9 ions·cm^{-2}·s^{-1}. A homogeneity of the response about 6% was found over the sensitive region with a well-defined confinement of the response within the active area. Tests of the radiation damage effect were performed by selectively irradiating small areas of the device with different ion fluences, up to about 10^{12} ions/cm^2. An exponential decrease of the charge collection efficiency was observed with a characteristic decay constant of about 4.8 MGy and 1 MGy for C and Si ions, respectively. The experimental data were analyzed by means of GEANT4 Monte Carlo simulations. A direct correlation between the diamond damaging effect and the Non Ionizing Energy Loss (NIEL) fraction was found. In particular, an exponential decay of the charge collection efficiency with an exponential decay as a function of NIEL is observed, with a characteristic constant of about 9.3 kGy-NIEL for both carbon and silicon ions. © *2015 AIP Publishing LLC*. [http://dx.doi.org/10.1063/1.4935525]

I. INTRODUCTION

Ion-beam therapy provides excellent dose conformity to the volume of deep-seated tumors,[1] sparing healthy tissues and avoiding organs at risk better than conventional therapy based on high energy photons. Moreover, heavy ions such as carbon ions offer an increased biological effectiveness in killing target tumor cells.[2]

The reference physical quantity adopted in order to estimate the biological effects induced by the radiation to the tissues is the absorbed dose, defined as the absorbed radiation energy per unit mass. However, for heavy ions, the only absorbed dose value is not sufficient to fully describe the biological effectiveness of the radiation. To this purpose, it is necessary to introduce the concept of radiation quality that depends on the particle type and energy spectrum.[3] Indeed, in ion-beam therapy, the radiation quality varies consistently as the particles slow down and/or produce secondary fragments.

A more detailed description of the radiation effectiveness can be achieved by the measurement of microscopic dosimetric quantities, allowing to determine the local radiation quality.[4] To this purpose, microdosimetric systems have been developed to provide the spectrum of the lineal energy, defined as the energy imparted to the micrometric volume by the impinging particles divided by the mean chord length of the active volume. The spectra of the lineal energy together with the value of the absorbed dose at the same point can be thus used to predict the response of the irradiated cells.[5] Therefore, microdosimeters are important tools which complement conventional dosimetry for preparing and performing ion-beam radiation therapy.[6,7]

An ideal microdosimeter must have a micrometric sensitive volume (actual or simulated) made of tissue-equivalent materials, should be able to cope with high ion fluxes and fluences, exhibiting a high energy resolution and an adequate radiation hardness. Among other solid state detectors, microdosimeters based on chemical vapor deposition (CVD) single-crystal diamond have been recently proposed and previously tested with alpha-particles and neutron radiation.[8] The prototypes are based on a layered p-type highly doped diamond/nominally intrinsic diamond/Schottky contact configuration.[9] The adopted structure allows to obtain very thin active volumes and to work without bias applied voltage. In addition, these devices are carbon made, thus providing high equivalence to human tissue as compared to other solid-state microdosimeters.

The use of diamond detectors in microdosimetry of ion-beam radiation therapy requires a detailed knowledge of the

response of such devices under different ion fluences and at different integrated doses. To this purpose, it is particularly relevant to analyze the response to few MeV ions, which are representative for therapeutic beams at the end of their penetration path, thus in the proximity of the distal border of the tumor.

In this work, a diamond based Schottky diode detector has been fabricated and characterized by means of Ion Beam Induced Charge (IBIC) technique at Ruđer Bošković Institute (RBI) microbeam facility[10] in order to assess the potentiality of such a device for ion-beam radiation therapy microdosimetry. Few MeV silicon and carbon ions were used to investigate both the device spectroscopic properties and the induced radiation damage effects. The presented results are analyzed in terms of Monte Carlo simulations in order to achieve a better understanding of the radiation damage induced in diamond.

II. DIAMOND BASED MICRODOSIMETER

The diamond microdosimeter was fabricated in a multilayered structure obtained by a three step deposition process. The structure of the diamond based microdosimeter and a picture of the wire bonded surface electrode are shown in Fig. 1. A highly conductive homoepitaxial boron doped diamond layer was deposited by microwave plasma-enhanced CVD on a $3 \times 3 \times 0.3\,mm^3$ high-pressure/high-temperature type Ib ⟨100⟩ single crystal diamond substrate. Such p-doped layer was used as a back contact. The boron concentration was estimated by the R-T curves, obtaining a value of the order of $10^{20}\,cm^{-3}$. A nominally intrinsic diamond layer was then grown on the doped one and used as the sensitive/active layer. The nominally intrinsic layer (roughly $0.5\,\mu m$ thick) was deposited in a separate CVD reactor. The diamond surface was then oxidized by isothermal annealing at 500 °C for 1 h in air, in order to remove the hydrogenated surface conductive layer. In Ref. 9, it has been shown that the nominally intrinsic layer acts as a slightly p-type doped layer with a concentration of acceptor of the order of $10^{14}\,cm^{-3}$.

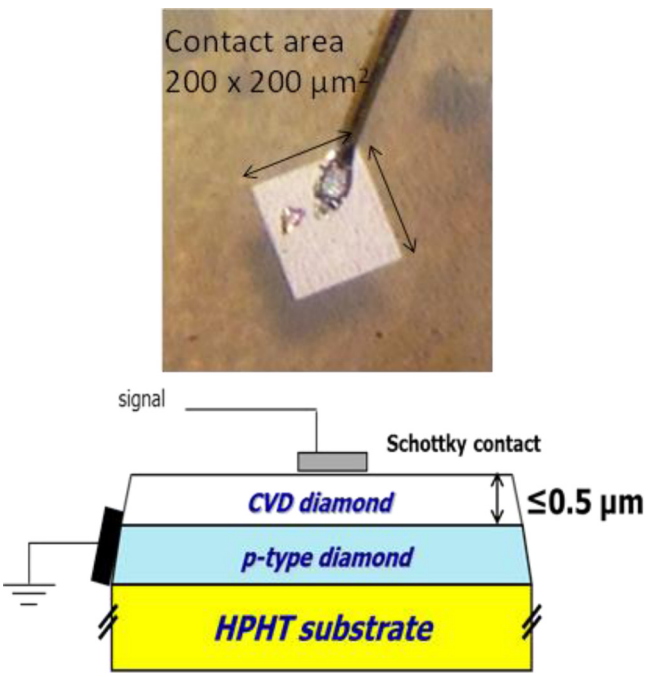

FIG. 1. Schematic representation of the diamond based microdosimeter and optical image of the Schottky metallic contact.

An aluminum contact, about 50 nm thick, was patterned on the diamond surface by a standard lift-off photo-lithographic technique and thermal evaporation. The Al electrode has a square shape of $200 \times 200\,\mu m^2$ in size. Finally, the detector was glued to Printed Circuit Boards (PCBs), which served as a sample holder and provided the electrical connection to the readout electronics through an SMA connector. Annealed silver paint was used to provide an ohmic contact to the B-doped layer while a $25\,\mu m$ Al wire was used to bond the Al electrode to the conducting trace of the PCB.

The adopted detector structure acts as a sandwich-type metal/p/p+ Schottky barrier diode, so that the device is able to operate without any external bias voltage as a result of its internal junction electric field.[9] All measurements reported in the present paper were performed with no external bias voltage applied.

III. DEVICE PRELIMINARY CHARACTERIZATION

The diamond based microdosimeter was preliminarily characterized under irradiation of 5.5 MeV α-particles from ^{241}Am source by using a calibrated electronic chain made by an ORTEC 142 A charge preamplifier, an ORTEC 672 spectroscopy amplifier, and a multichannel analyzer. The spectra were acquired in vacuum.

The stability of the response was first verified by performing a 12 h α-particles irradiation and by comparing the spectra acquired at different times. The detector response was found stable and reproducible with no evidence of polarization effects.

For a correct evaluation of the device operation in microdosimetry field, the precise sensitive diamond layer thickness must be known. This evaluation was performed by analyzing the detector response to α-particles from a collimated ^{241}Am source as a function of the incidence angle between the beam direction and the normal to the detector surface. Two typical spectra, collected at two different angles, are shown in Fig. 2(a). The peak channel positions were then converted to energy values and displayed as function of the impinging angles in Fig. 2(b). An increase of detected energy with the impinging angle value can be clearly noticed, due to the increased α-particles path inside the active diamond layer.

By assuming an homogeneous response of the detector, the sensing layer thickness can be evaluated as follows: the Bragg curve of 5.5 MeV α-particles in diamond has been calculated by the nuclear simulation program SRIM[11] and approximated to the empirical function $\xi_{loss}(x)$ expressed in (MeV/μm)[12]

$$-\frac{dE}{dx} \approx \xi_{loss}(x) = \frac{Ae^{Bx}}{1+e^{x-C/D}}, \quad (1)$$

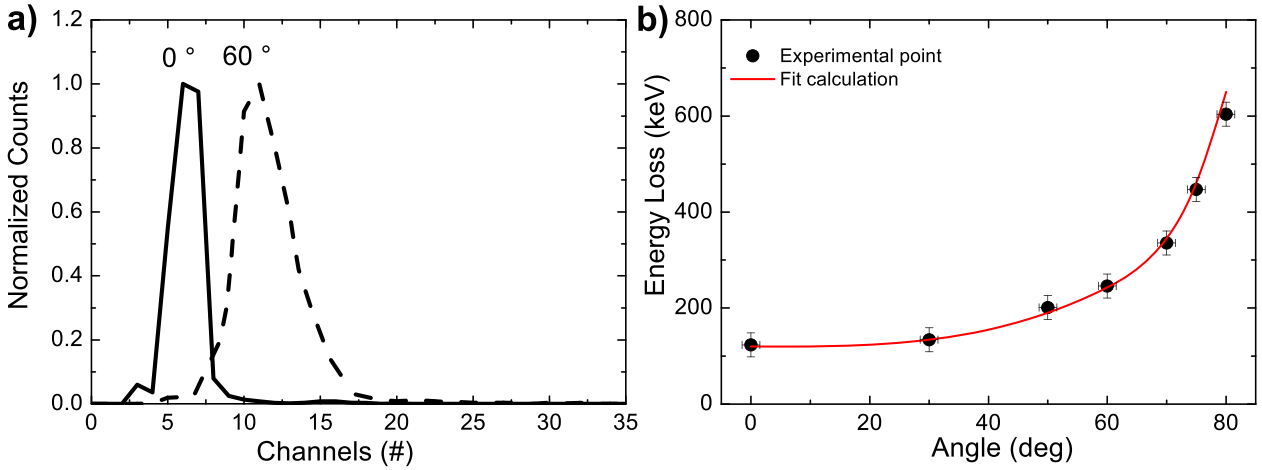

FIG. 2. (a) Collected spectra for α particles impinging on the diamond detector at different incidence angles. (b) Experimental values of energy loss of alpha particle in the diamond active layer as a function of incidence angle. Simulated curve based on SRIM calculation is also reported (solid line).

x being the abscissa along the direction of propagation of the impinging particle. The four parameters A, B, C and D have been derived from the best fit of Eq. (1) to the calculated Bragg curves. By neglecting straggling effects, the distance travelled by the impinging particle within the sensitive thickness is d/cos(θ), where d is the detection region thickness and θ the incident angle. The collected energy is therefore given by

$$E_c(\theta) = \int_0^{d/\cos(\theta)} \xi_{\text{loss}}(x)\, dx. \qquad (2)$$

The best fit of Eq. (2). with the experimental data was numerically calculated and reported in Fig. 2(b) (solid line). From the resulting value of the fit parameters, a thickness of about $0.43 \pm 0.05\ \mu$m has been estimated.

In order to verify such active diamond thickness, the depletion region width of the Schottky junction, which extends below the metallic contact within diamond layer, Capacitance-Voltage (C-V) measurements were performed by using an Agilent inductance, capacitance, resistance meter 4284A. The junction capacitance of the devices is approximated to that of a parallel plate capacitor so that the depletion thickness W of the detector was estimated by the following equation $W = \varepsilon_0 \varepsilon_r A/C$, where A is the area of the square contact, ε_o dielectric constant of free space, and ε_r dielectric constant of the diamond. A depletion thickness of about $0.4 \pm 0.04\ \mu$m was obtained, which is compatible with the sensitive diamond film thickness, previously estimated.

IV. MICRO-BEAM EXPERIMENTAL SET-UP

The diamond based microdosimeter has been tested at the Ruđer Bošković Institute ion microprobe facility. The ions were accelerated by a 6 MV Tandem Van de Graaff accelerator. The calibration of the beam position in micrometers was made scanning the microbeam over a silicon diode with a copper wire mask with calibrated micrometric mesh positioned on top of it. The spot size of the focused ion beam was approximately 1 μm.

The diamond microdosimeter was connected to a conventional charge-sensitive electronic chain, consisting of a charge-sensitive preamplifier ORTEC 142A and an ORTEC 570 shaping amplifier. The shaping time of the amplifier was set to 0.5 μs. Pulse high spectra for the incident ions were measured using an analog to digital multichannel analyzer CAMBERRA 8075.

The pressure in the vacuum chamber was of the order of 10^{-7} mbar. However, in some regions of the vacuum tube prior to the microbeam focussing lenses, it was of the order of 10^{-5} mbar. Although this pressure was sufficient to keep energy loss induced by collisions with residual gas molecules negligible, such collisions can produce some small angle scattering events which are responsible for a beam halo in the IBIC images. Pulse height processing, beam scanning, and 2D map acquisition were carried out by using the Spector data acquisition software, developed at the RBI.[10] The electronic chain was calibrated using a silicon detector and a precision pulse generator, in order to compare pulse heights provided by the reference Si detector with those from the diamond device.

Two different ions were used, i.e., 5 MeV silicon ions and 4 MeV carbon ions. As simulated by the SRIM code, 5 MeV Si ions and 4 MeV C ions have a penetration depth in diamond of approximately 1.5 μm and 2.0 μm, respectively, allowing the ions to cross the diamond sensitive region.

The scanned microbeam was used for two different purposes:

- the IBIC scanning process, characterized by low flux (about 10^7 ions·cm^{-2} s^{-1}) in order to assess the diamond microdosimeter response in terms of the charge transport properties at microscopic level with high spatial resolution.
- radiation-induced damage tests, characterized by high flux (up to 1.7×10^9 ions·cm^{-2} s^{-1}), for delivering homogeneous number of particles over a defined cross area of the diamond sample.

In the latter case, for each ion type, four different selective areas were irradiated by scanning the focused beam and

varying the ion fluence within 10^{10} and 10^{12} ions·cm^{-2}. The size of each irradiated area was $11.5\,\mu m \times 11.1\,\mu m$ and $17.7\,\mu m \times 17.1\,\mu m$ for Si and C ions, respectively. The amount of impinging ions and the value of the calculated fluence for the different irradiated areas are reported in Table I. After irradiations that produced selectively damaged regions in the diamond detector, IBIC microscopy has been performed to measure the degradation of the charge collection efficiency. The different damaged areas corresponding to the lower charge collection efficiency are clearly visible in the bottom of Fig. 3 for both ions.

V. RESULTS AND DISCUSSION

A. IBIC characterization

Fig. 3 shows the IBIC map collected from diamond detector showing a quite uniform sensitivity, well confined inside the $200\,\mu m \times 200\,\mu m$ metallic contact. This implies that a clear current signal is induced by the drift of charge carriers in the depletion region surrounding the sensitive electrode, whereas free carriers generated elsewhere do not induce detectable signals. The isolated events recorded in pixels outside the square pad correspond to the beam halo effect. In circumstances similar to those used in this experiment, the microbeam profile is of Lorenzian shape with tail (halo) extending to several tens or even hundreds of micrometers.[13] This is, in particular, observed in low current microbeam techniques such as IBIC. The recorded counts outside the sensitive detector area are mainly due to the particles that are scattered on residual gas molecules in the beam line tubes. In this case, these events represent from 3% to 6% of the total detected events. Due to the asymmetric demagnification of the microprobe focusing system, higher concentration of "halo" is in horizontal, low demagnification plane. The Al wire bonding is responsible for the lack of events at the top of the square pad, as clearly visible in Fig. 3. The Al wire is thick enough (25 μm Al) to fully stop the ions before entering in the diamond sensitive volume. A second small blind region is also observed on the left side of the IBIC map. This is due to an Al wire fragment accidentally deposited on the electrode during the micro welding procedure (see Fig. 1(a).

The response of the microdosimeter was found stable, with variation of the peak position of the charge collection efficiency (CCE) spectra over a time interval of 150 min below $\pm 0.2\%$.

TABLE I. Fluence values of IBIC tests with 5 MeV silicon and 4 MeV carbon ions.

IBIC test name	Impinging ions (#)	Fluence (ions/cm^2)
Si-a	412 450	3.2×10^{11}
Si-b	195 771	1.5×10^{11}
Si-c	102 551	8.4×10^{10}
Si-d	49 390	3.9×10^{10}
C-a	5 050 545	1.7×10^{12}
C-b	2 256 279	7.4×10^{11}
C-c	1 108 114	3.6×10^{11}
C-d	533 769	1.8×10^{11}

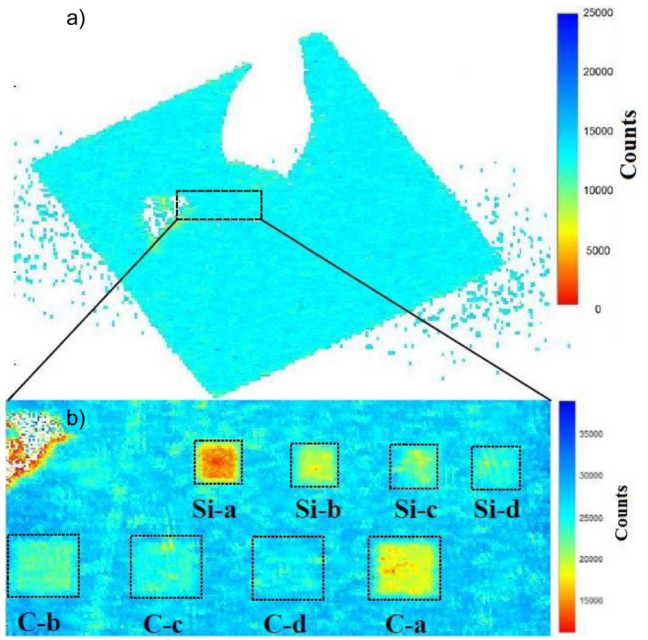

FIG. 3. (a) IBIC pulse height 2D distribution measured over the whole sensitive square area of the diamond detector. (b) IBIC scan performed with 4 MeV carbon ions showing the previously irradiated areas with 5 MeV silicon ions and 4 MeV carbon ions.

The uniformity of the response was quantified studying the distribution of the CCE for over a large portion of the detector surface. From the IBIC scanning of the detector surface with carbon ions, the mean signal amplitude at each irradiated pixel was calculated. The standard deviation of the mean signal distribution over the sampled pixels provides a 6% homogeneity of the detector response.

In order to evaluate the broadening of the response at the edge of the contact, thus the capability of such a device to define a precise sensitive area, a profile of the signal at the edge of contact is reported in Fig. 4(a). The charge collection efficiency shows a constant trend inside the contacted area and diminishes abruptly as the beam is outside the contact pad according to the strength of the internal electric field. From the full width at half maximum (FWHM) of the Gaussian fit of the derivative of the experimental data, an edge broadening of about 0.8 μm is obtained (see Fig. 4(b). This value is comparable to the size of the beam spot demonstrating a high definition capability of diamond Schottky diode devices. In particular, such a spatial definition is much higher than the one reported for microdosimeters based on metal-insulator-metal (MIM) configuration,[14] allowing to further optimize the device geometry for specific microdosimetric application.

B. Radiation damage

The radiation damage effect was studied by irradiating under high ions flux condition eight small specific areas (see bottom of Fig. 3). The ions' fluence for each specific area is reported in Table I.

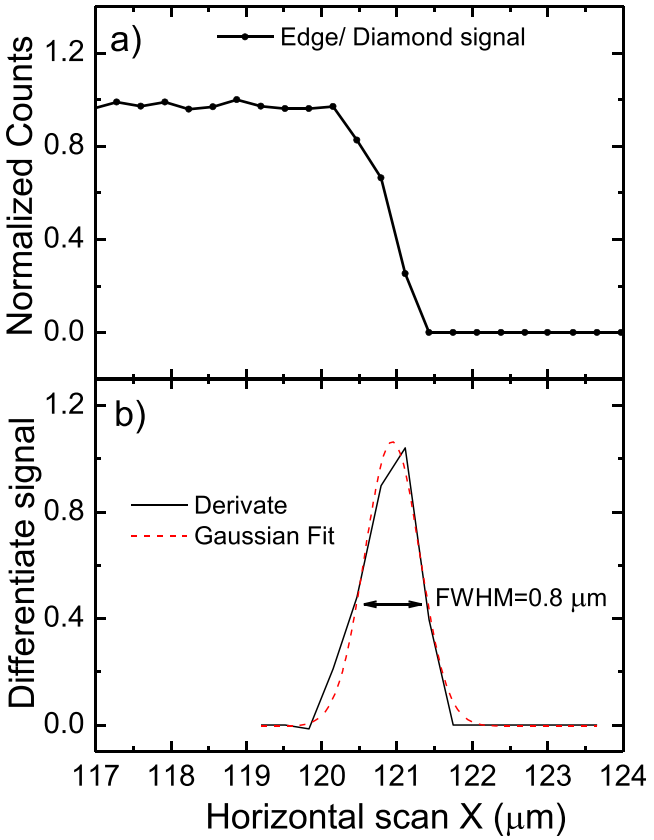

FIG. 4. (a) Profile of the signal measured at the edge of the metal contact along the X-direction. (b) Derivative of the experimental data (full line) and its Gaussian best fit curve (dashed line).

The eventual presence of polarization effects or persistence behaviors of the detector response[15,16] has been firstly verified. This was done by comparing the spectra acquired during the damaging procedure in high-flux conditions to the ones collected at low-flux after approximately 1 h delay time. In Fig. 5, 4 MeV carbon ions normalized spectra relative to three selective areas are shown. For each irradiated

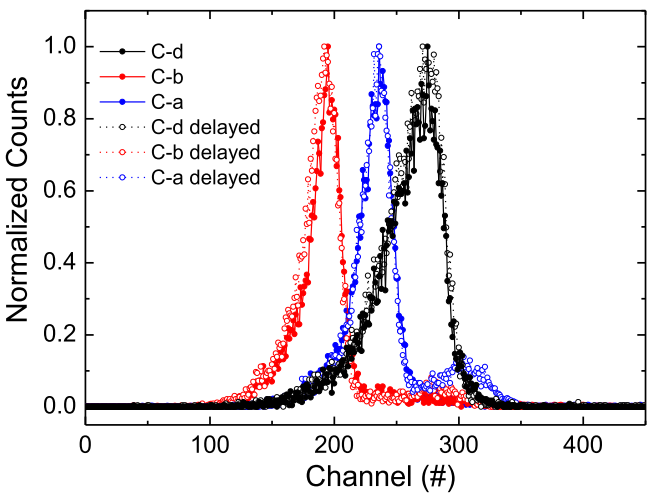

FIG. 5. 4 MeV carbon ions normalized spectra relative to three selective areas measured both during final sequence of the irradiation procedure (full dots) and during the delayed low-beam current scans (open dots).

TABLE II. Effects on diamond deterioration due to accumulated dose from 4 MeV carbon ion, estimated by two IBIC scanning processes performed at different delay times from the irradiation.

C fluence (ions/cm^2)	No delay (C-probe) Peak position	1 hour delay (C-probe) Peak position	Relative difference
$1.7\cdot10^{12}$	193.8	190.8	1.50%
$7.4\cdot10^{11}$	234.3	234.4	0.21%
$3.6\cdot10^{11}$	252.6	252.1	−0.20%
$1.8\cdot10^{11}$	270.8	267.8	0.42%

area, two spectra are reported accounting for the same amount of particles (i.e., 12 000 ions). The solid dots correspond to spectra collected during the final sequence of the radiation-induced damage procedure for each specific area while the open circles correspond to the delayed low-flux scans over the same irradiated areas. The smaller peak noticeable at high channel values (see spectra "C-a delayed" of Fig. 5) is due to particles that are scattered by residual gas molecules (halo effect) towards undamaged areas of the detector and erroneously attributed to the region of interest. The comparison between the peak position values calculated for each carbon ion spectrum is reported in Table II. The maximum difference between the peak position measured under high-flux (no delay) and low-flux (1 h delay) condition is below 1.5%, indicating the absence of polarization effects and the capability of diamond Schottky diodes to operate under high flux rate. Such a behavior differs from that reported in the literature for MIM diamond detectors where a strong dependence of the detector response as a function of the count rate and the ionization density has been observed.[17,18]

A similar analysis was performed for 5 MeV silicon ions irradiation. In this case, the response of each irradiated area was measured in the three different conditions: IBIC scanning with 5 MeV silicon ions under high-flux condition, low-flux IBIC scanning with 5 MeV silicon ions delayed by approximately 30 min, and IBIC scanning with 4 MeV carbon ions delayed by about one day. The peak positions in these three cases for different fluences are reported in Table II. The differences between high-flux and delayed low-flux spectra are more evident than in the case of carbon ions. The disagreement could arise from the smaller number of events collected in low flux conditions (5000 ions) leading to a larger uncertainty. On the other hand, the relative differences exhibit alternate signs, suggesting that no polarization effects occur. In order to compare the previously mentioned response under Si ions to the one obtained 20 h later with C ions on the same areas, the C-ions peak positions were properly scaled to the Si-ions ones. This was done by multiplying the C-ions peak position values by the ratio between the response under 5 MeV silicon and 4 MeV carbon as measured in an undamaged area. The results are also reported in Table III, where a significant agreement with the silicon irradiation can be appreciated with variation below 1%. It should be noticed that in such a case, the same number of events of the data reported in Table II (i.e., 12 000 ions) was taken into account, producing a higher statistic with respect to the case of Si ions probe.

TABLE III. Dependence of CCE on dose accumulation produced by 5 MeV silicon ion at different time delays.

Si fluence (ions/cm^2)	No delay (Si-probe) Peak position	$^1/_2$ hour delay (Si-probe) Peak position	Relative difference	20 hour delay(C-probe) Peak position	20 hour delay (C-probe) scaled peak position	Relative difference
$3.2{\cdot}10^{11}$	47.61	48.48	1.79%	149.85	47.57	−0.08%
$1.5{\cdot}10^{11}$	63.35	59.39	−6.67%	200.87	63.76	0.64%
$8.4{\cdot}10^{10}$	73.72	72.36	−1.88%	234.23	74.33	0.82%
$3.9{\cdot}10^{10}$	79.8	81.03	1.52%	251.37	79.79	−0.02%

The effect of the radiation damage as a function of the ion fluence is reported in Fig. 6(a)), where the CCE values for each damaged area were extracted from the low-beam current IBIC measurement using 4 MeV carbon ions probe. The persistence with time of the lowered efficiency observed in the highly irradiated area indicates the occurrence of permanent damage due to radiation induced lattice defects. In addition, the absence of polarization effects under high-flux condition makes possible to evaluate the CCE decrease also from the data acquired during the damaging irradiation run. Such an analysis condition was performed in order to estimate the vertical error bars reported in Fig. 6. In particular, each value reported in Fig. 6 was compared to the ones obtained by analyzing proper segments extracted from all the damaging acquisition runs corresponding to the same ion fluence.

The uncertainty on the particle fluence (horizontal error bars) is mainly related to the determination of sizes of the irradiated areas. Those were estimated performing IBIC scans interposing a copper mask with calibrated micrometric mesh.

In Fig. 6(b)), the normalized CCE values are reported as a function of the absorbed dose. The total dose accumulated on the diamond (horizontal axis scale) has been derived for each particle type from the particle fluence value by using Monte Carlo Geant4-based simulation (release 4.9.5.p01).[19,20] An exponential decay of the CCE is observed in Figs. 6(a) and 6(b)), where the best fit curves calculated using the equation $f(x) = e^{-x/\tau}$ are also reported (dashed lines). The obtained results for the τ parameter are reported in Table IV.

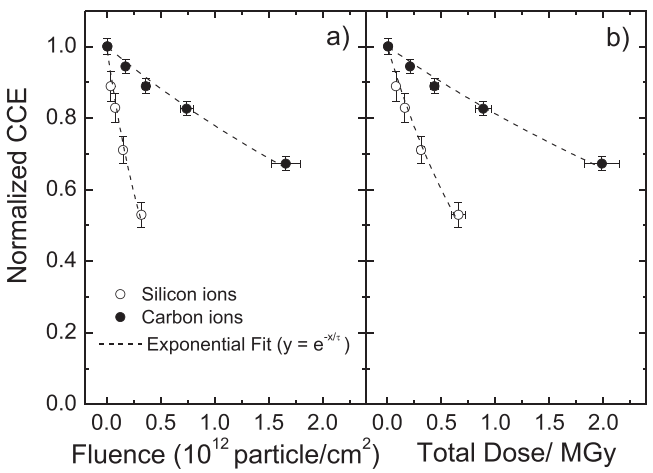

FIG. 6. Normalized CCE as a function of the fluence (a) and as function of the total absorbed dose (b), both for 5 MeV silicon ions and 4 MeV carbon ions. The best fit curves, calculated with a one-parameter exponential decay function, are also reported.

Comparing these results to the typical dose values adopted in ion-beam therapy, a CCE decrease of 1% is expected when the detector is exposed a dose corresponding to the full treatment of about two thousand patients. It is worth to notice that the observed radiation tolerance of the proposed diamond Schottky diode is more than one order of magnitude higher than one obtained in MIM diamond based detectors irradiated in similar conditions.[21] This behavior is believed to originate from the very small thickness of active diamond layer in the Schottky diode configuration as compared with the thicknesses of MIM devices. Indeed, the defect density introduced by the irradiation procedure produces a decrease of the carrier lifetime and of the charge collection distance. The consequent CCE reduction is then less effective in thinner active layer where a smaller drift distance is traveled by the carriers.

As evident from Fig. 6(b), a much higher radiation damage is induced by Si ions with respect to C ions when the detector is exposed to the same dose level. Such behavior can be accounted for by analyzing in more detail the damage process induced by the radiation. The radiation damage in the detector is related to the nucleus-nucleus interactions dominated at low energies by elastic scattering mechanisms. This produces target nuclei recoil that can result in a displacement of the nucleus from the diamond crystal lattice. The energy per unit path lost by the incident particle due to displacement processes is called Non Ionizing Energy Loss (NIEL) and it depends on the projectile nucleus atomic number and energy, and on the target nuclei. The NIEL yields a number of point defects that depend on the displacement threshold of diamond crystal, which is in the range 37–47 eV (depending on the crystallographic direction[22,23]). The NIEL fraction of carbon and silicon ions has been estimated through Monte Carlo Geant4-based simulations. The irradiated device was modeled as a 430 nm thick diamond disk covered by 50 nm thick aluminum contact. The standard electromagnetic physics is employed, simulating ion energy

TABLE IV. Characteristic decay constants obtained from exponential function fit of CCE values as a function of fluence, absorbed dose and NIEL fraction for carbon and silicon ions.

	$\tau_{fluence}$ (ions/cm$^2 \times 10^{12}$)	τ_{dose} (MGy)	τ_{NIEL} (kGy)
C	4.0 ± 0.2	4.8 ± 0.2	9.4 ± 0.5
Si	0.48 ± 0.02	0.98 ± 0.05	9.3 ± 0.4

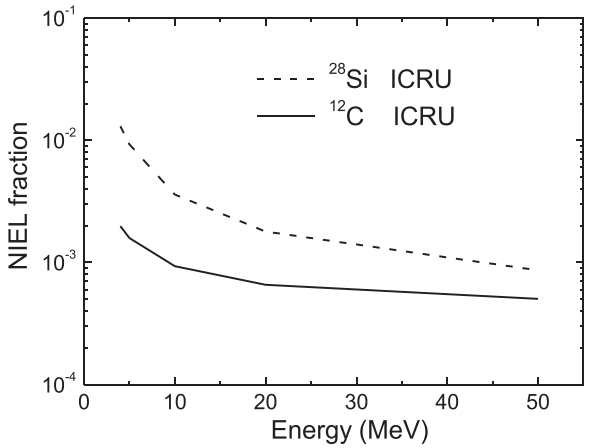

FIG. 7. NIEL fraction computed for carbon ions (solid line) and silicon ions (dash line) as a function of the ions energy.

loss and its fluctuation, based on ICRU 49 stopping powers.[24]

The calculated NIEL fraction, defined as the ratio between the NIEL dose and the total absorbed dose in the diamond active layer, is reported in Fig. 7 as a function of the ion energy for both carbon and silicon ions. A much higher NIEL fraction is obtained in the case of silicon ion. This is in agreement with the higher radiation damage capability of Si ions noticeable in Fig. 6. The normalized CCE as a function of the estimated NIEL dose is shown in Fig. 8. The best fit curves calculated with a one parameter exponential function are also reported in Fig. 8 for both silicon and carbon ions. The values of the obtained characteristic decay constants τ_{NIEL} are reported in Table IV. It is worth to notice that Si and C ions CCE data are overlapped within the experimental uncertainty, suggesting a clear correlation between the diamond aging and the NIEL. In particular, a very good agreement between the calculated τ_{NIEL} values for C and Si ions was found, with a relative difference of about 1.1%. Such result indicates that the radiation damage can be directly correlated to the non-ionizing fraction of the energy loss in the diamond crystal, allowing to predict the CCE decrease for different energies and ion types.

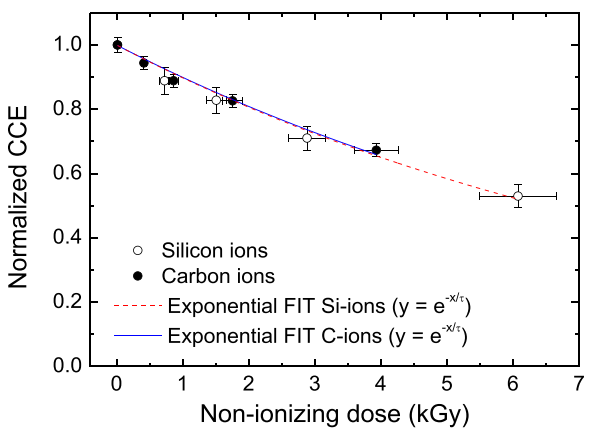

FIG. 8. Normalized CCE as a function of the dose due to non-ionizing energy loss (NIEL). The best fit curves, calculated with an exponential function, are also reported.

VI. CONCLUSIONS

Carbon and silicon focused ion microbeams were used to investigate the properties of a thin diamond based detector for microdosimetric applications in ion-beam therapy. A stable response with no evidence of polarization effects was observed up to the maximum ion beam flux investigated (about 1.7×10^9 ions/cm^2·s). Measured IBIC maps have evidenced a homogeneity of about 6% over a large portion of the sensitive region with a well-defined confinement of the response within the active area. This result indicates a high definition capability of diamond Schottky diode response, leading to the possibility of producing innovative microdosimeter with optimized performance.

Radiation tolerance tests were performed by massively irradiating specific areas of the device. The device showed high radiation tolerance capabilities, being able to cope with ion fluences well beyond the ones typically adopted in ion beam therapy facilities. Thanks to the very small thickness of the active diamond layer in the proposed Schottky diode; its radiation tolerance was found to be more than one order of magnitude higher than that obtained in standard diamond based detectors (MIM) irradiated in similar conditions. The experimental results of the radiation damage test were also analyzed by means of GEANT 4 Monte Carlo simulation, by calculating the NIEL fraction of the impinging ions inside the diamond lattice. A direct correlation between the diamond aging and the NIEL fraction was found. In particular, an exponential decay of the CCE as a function of NIEL was observed with a characteristic decay constant of about 9.3 kGy-NIEL for both carbon and silicon ions. Such a result clearly indicates the possibility of predicting the induced radiation damage in diamond based Schottky diodes for different incident ion types and energy.

[1]R. R. Wilson, Radiobiology **47**, 487–491 (1946).
[2]J. S. Loeffler and M. Durante, Nat. Rev. Clin. Oncol. **10**, 411–424 (2013).
[3]International Atomic Energy Agency and International Commission on Radiation Units and Measurements, Relative Biological Effectiveness in Ion Beam Therapy, Technical Reports Series No. 461, Jointly sponsored by the IAEA and ICRU, Vienna (2008), available at: http://www-pub.iaea.org/MTCD/publications/PDF/trs461_web.pdf.
[4]H. H. Rossi, Radiat. Res. **10**, 522–531 (1959).
[5]L. De Nardo, V. Cesari, N. Iborra, V. Conte, P. Colautti, J. Herault, G. Tornielli, and P. Chauvel, Phys. Med. **XX**(2), 71–77 (2004).
[6]International Commission on Radiation Units and Measurements, Microdosimetry, ICRU Report 36, Woodmont Avenue, Bethesda, Maryland, 20814, USA, 1983.
[7]G. Magrin and R. Mayer, Mod. Phys. Lett. A **30**, 1540027 (2015).
[8]S. Rollet, M. Angelone, G. Magrin, M. Marinelli, E. Milani, M. Pillon, G. Prestopino, C. Verona, and G. Verona-Rinati, IEEE Trans. Nucl. Sci. **59**, 2409–2415 (2012).
[9]S. Almaviva, M. Marinelli, E. Milani, G. Prestopino, A. Tucciarone, C. Verona, G. Verona-Rinati, M. Angelone, M. Pillon, I. Dolbnya, K. Sawhney, and N. Tartoni, J. Appl. Phys. **107**, 014511 (2010).
[10]M. Jakšić, I. B. Radović, M. Bogovac, V. Desnica, S. Fazinić, M. Karlušić, Z. Medunić, H. Muto, Ž. Pastuović, Z. Siketić, N. Skukan, and T. Tadić, Nucl. Instrum. Methods Phys. Res. B **260**, 114–118 (2007).
[11]J. F. Ziegler, M. D. Ziegler, and J. P. Biersack, Nucl. Instrum. Methods Phys. Res. B **268**, 1818 (2010).
[12]S. Almaviva, M. Marinelli, E. Milani, G. Prestopino, A. Tucciarone, C. Verona, G. Verona-Rinati, M. Angelone, D. Lattanzi, M. Pillon, R. M. Montereali, and M. A. Vincenti, J. Appl. Phys. **103**, 054501 (2008).
[13]T. Tadić and M. Jakšic, Nucl. Instrum. Methods Phys. Res. B **267**, 2028–2031 (2009).

[14]J. A. Davis, K. Ganesan, A. D. C. Alves, D. A. Prokopovich, S. Guatelli, M. Petasecca, M. L. F. Lerch, D. N. Jamieson, and A. B. Rosenfeld, IEEE Trans. Nucl. Sci. **61**, 3479–3484 (2014).
[15]D. S. Bale and C. Szeles, Phys. Rev. B **77**, 035205 (2008).
[16]C. Manfredotti, A. Lo Giudice, E. Vittone, F. Fizzotti, Y. Garino, and E. Pace, Diamond Relat. Mater. **15**, 1467–1471 (2006).
[17]V. Grilj, N. Skukan, M. Jakšic′, W. Kada, and T. Kamiya, Nucl. Instrum. Methods Phys. Res. B **306**, 191–194 (2013).
[18]Y. Sato, T. Shimaoka, J. H. Kaneko, H. Murakami, M. Isobe, M. Osakabe, M. Tsubota, K. Ochiai, A. Chayahara, H. Umezawa, and S. Shikata, Nucl. Instrum. Methods Phys. Res. A **784**, 147 (2015).
[19]S. Agostinelli *et al.*, Nucl. Instrum. Methods Phys. Res. A **506**, 250–303 (2003).
[20]J. Allison *et al.*, IEEE Trans. Nucl. Sci. **53**, 270–278 (2006).
[21]I. Zamboni, Ž. Pastuović, and M. Jakšić, Diamond Relat. Mater. **31**, 65–71 (2013).
[22]J. Koike, D. M. Parkin, and T. E. Mitchell, Appl. Phys. Lett. **60**, 1450 (1992).
[23]M. Pillon, M. Angelone, G. Aielli, S. Almaviva, M. Marinelli, E. Milani, G. Prestopino, A. Tucciarone, C. Verona, and G. Verona-Rinati, J. Appl. Phys. **104**, 054513 (2008).
[24]A. Allisy *et al.*, "Stopping powers and ranges for protons and alpha particles," ICRU Report 49 (1993).